materials

MDPI

Article

Effect of Hydrogen Exposure on Mechanical and Tribological Behavior of Cr_xN Coatings Deposited at Different Pressures on IN718

Aleksei Obrosov [1,*], Alina N. Sutygina [2], Alex A. Volinsky [3], Anton Manakhov [4], Sabine Weiß [1] and Egor B. Kashkarov [2]

1 Chair of Physical Metallurgy and Materials Technology, Brandenburg Technical University, Cottbus 03046, Germany; sabine.weiss@b-tu.de
2 Department of General Physics, National Research Tomsk Polytechnic University, Tomsk 634050, Russia; sutygina2013@mail.ru (A.N.S.); egor_kashkarov@mail.ru (E.B.K.)
3 Department of Mechanical Engineering, University of South Florida, Tampa, FL 33620, USA; volinsky@usf.edu
4 Laboratory of Inorganic Nanomaterials, National University of Science and Technology "MISiS", Moscow 119049, Russia; ant-manahov@ya.ru
* Correspondence: aleksei.obrosov@b-tu.de; Tel.: +49-355-694-251

Academic Editor: Silvia Gross
Received: 28 March 2017; Accepted: 12 May 2017; Published: 20 May 2017

Abstract: In the current study, the properties of the Cr_xN coatings deposited on the Inconel 718 superalloy using direct current reactive magnetron sputtering are investigated. The influence of working pressure on the microstructure, mechanical, and tribological properties of the Cr_xN coatings before and after high-temperature hydrogen exposure is studied. The cross-sectional scanning electron micrographs indicate the columnar structure of the coatings, which changes from dense and compact columns to large columns with increasing working pressure. The Cr/N ratio increases from 1.4 to 1.9 with increasing working pressure from 300 to 900 mPa, respectively. X-ray diffraction analysis reveals a change from mixed hcp-Cr_2N and fcc-CrN structure to approximately stoichiometric Cr_2N phase. After gas-phase hydrogenation, the coating deposited at 300 mPa exhibits the lowest hydrogen absorption at 600 °C of all investigated coatings. The results indicate that the dense mixed cubic and hexagonal structure is preferential for hydrogen permeation resistance due to the presence of cubic phase with higher packing density in comparison to the hexagonal structure. After hydrogenation, no changes in phase composition were observed; however, a small amount of hydrogen is accumulated in the coatings. An increase of coating hardness and elastic modulus was observed after hydrogen exposure. Tribological tests reveal that hydrogenation leads to a decrease of the friction coefficient up to 20%–30%. The best value of 0.25 was reached for hydrogen exposed Cr_xN coating deposited at 300 mPa.

Keywords: Cr_xN coatings; PVD; hydrogenation; tribology; mechanical properties; GDOES

1. Introduction

Since the commercialization of TiN coatings in 1980s, transition metal nitride hard coatings have been extensively applied in bearings, gears, as well as cutting and forming tools because of their high hardness, good wear, and corrosion resistance [1,2]. Their capability to extend tool lifetime in abrasive and corrosive environments has been verified [3].

Chromium nitride coatings exhibit higher corrosion and oxidation resistance in comparison to other nitride coatings [4,5]. Moreover, Cr–N coatings have attracted much attention in different

applications in terms of their high temperature stability, chemical inertness, high toughness, and a friction coefficient lower than TiN [6].

Cr–N coatings can be synthesized by various PVD processes, such as hollow cathode discharge [7], pulsed laser deposition [8,9], ion-beam-assisted deposition [10,11], arc ion plating [12–14], and magnetron sputtering [15–18].

Phase structure, morphology, and mechanical properties of Cr–N coatings deposited using magnetron sputtering strongly depend on the deposition parameters, such as working pressure, bias voltage, substrate temperature, target power, substrate frequency, nitrogen flow rate, etc. [4,18–21]. Among them, working pressure is one of the key parameters which controls the deposition process. Gas pressure directly affects phase structure, preferred orientation, chemical composition, and deposition rate of the coatings [22,23].

Application of Cr–N coatings and Inconel 718 (IN718) superalloy in the hydrogen-contained aggressive environments requires detailed knowledge about changes in physical and mechanical properties of the material during hydrogen interaction at elevated temperatures. According to literature, the presence of δ-phase in IN718 at high hydrogen concentrations dramatically reduces the ductility of the alloy [24]. Furthermore, hydrogen embrittlement of IN718 occurs preferably at the grain boundaries even at low hydrogen concentrations. Thus, developing hydrogen-resistant coatings with adequate mechanical and tribological properties on the IN718 alloy is also very important to prevent hydrogenation.

Despite numerous publications about Cr–N films, up to now the effect of hydrogenation on mechanical and tribological properties of Cr–N coatings has not been completely understood. The objective of this paper is to investigate the influence of the pressure on microstructure, mechanical, and tribological properties of Cr_xN coatings before and after high-temperature hydrogen exposure.

2. Experimental

Cr_xN coatings were fabricated using DC magnetron sputtering in the CC800/9 industrial coater from CemeCon AG (Würselen, Germany). The coatings were deposited onto IN 718 and (100) silicon wafers. IN 718 substrates were mirror polished, ultrasonically cleaned in acetone and ethanol, and then placed in the chamber at the substrate-to-target distance of 70 mm. For deposition of the coating, with the stationary table, the specimens were placed opposite to the target. A high purity, single Cr target (99.99%) from CemeCon AG (Würselen, Germany) was used. Prior to sputtering, a base pressure of less than 8.0 mPa was achieved in the chamber. Then the substrates were etched with Ar^+ plasma at a bias voltage of -650V for 30 min in order to remove surface contaminations and ensure proper adhesion of the deposited films. The coating temperature was kept constant through all experiments at 500 °C. The target power of 2 kW and substrate bias voltage of 90 V were kept constant. N_2/Ar ratio for all deposited coatings was 0.23. In this study, the working pressure was changed from 300 to 900 mPa.

The film thickness was measured using the CemeCon AG (Würselen, Germany) calowear test machine. The deposition rate was calculated from the film thickness and the corresponding deposition time. The cross-section images of the Cr_xN thin films deposited on Si wafers were analyzed by means of scanning electron microscope from Tescan (Brno, Czech Republic). The chemical composition of the Cr_xN layers was determined by wavelength-dispersive X-ray spectroscopy (WDS).

The hydrogenation was carried out in gas atmosphere using the Gas Reaction Controller (GRC) technique (Pittsburgh, PA, USA). Initially, the sample was placed into the vacuum chamber and evacuated to the base pressure of 10^{-3} Pa. Then, the sample was heated to 600 °C with a heating rate of 6 °C/min. Finally, the chamber (175 cm^3) was filled with hydrogen (99.999% purity) up to 2 atm pressure and kept for two hours. After hydrogenation, hydrogen was pumped out of the chamber during slow cooling. Elemental distribution was analyzed by glow-discharge optical emission spectroscopy (GDOES) using GD Profiler 2 (Horiba, Japan).

Crystallographic phases and XRD patterns of the coatings were identified using the Shimadzu XRD 7000S (Kyoto, Japan) equipped with the OneSight wide-range high-speed detector at 40 kV and 30 mA with CuK_α radiation (λ = 0.15406 nm). Nanohardness of the coatings was measured using the nanohardness tester NHT-S-AX-000X from CSEM (Neuchatel, Switzerland). This device analyzes changes in load and indenter penetration depth at the loading–unloading cycle using the Oliver and Pharr method [25]. The load was adjusted so that the penetration depth did not exceed one-tenth of the coating thickness [26]. The average of 20 measurements was calculated. The evolution of the friction coefficients was investigated by the high-temperature tribometer TNT-S-AH0000 from CSEM (Neuchatel, Switzerland) under dry friction conditions with a 5 N vertical load and a linear sliding speed of 2.5 cm/s for 15,000 laps (the total distance is approx. 150 m).

3. Results and Discussion

3.1. Morphology and Structural Analysis

The cross-sectional SEM micrographs of the Cr_xN coatings, deposited at various pressures are shown in Figure 1. It can be observed that the coating deposited at a low pressure (300 mPa) has a compact columnar microstructure with closely-packed columns. The increasing working pressure results in larger columns and higher porosity of the coating. Furthermore, a change in coating growth was observed. At a low pressure, the coating grows in approximately 65° direction with respect to the substrate, whereas the coating growth at 900 mPa was practically perpendicular to the substrate. Coating microstructure plays an important role in affecting mechanical and tribological properties as well as hydrogen permeation [18,27–30].

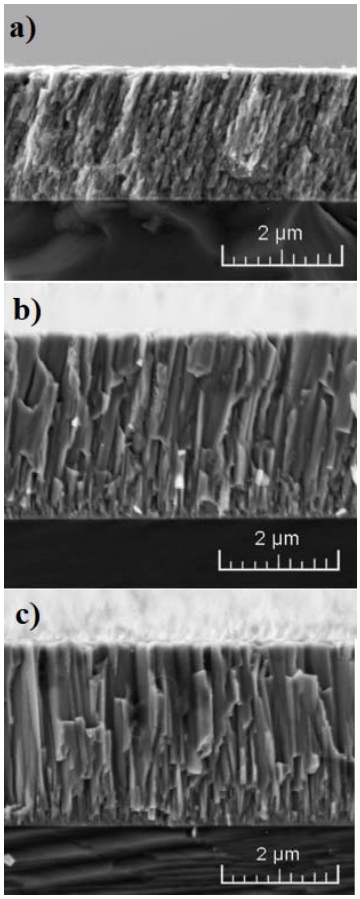

Figure 1. Cross-section SEM images of Cr_xN deposited at various pressures (**a**) 300 mPa; (**b**) 600 mPa; and (**c**) 900 mPa.

The WDS analysis shows that the Cr content increases from 59 at. % to 66 at. % with increasing pressure, while the nitrogen content decreases (Table 1). The Cr/N ratio changes from 1.4 to 1.9. At these compositions, according to the equilibrium phase diagram [31], a change from mixed CrN + Cr_2N to uniform Cr_2N can be expected.

An increasing coating deposition rate was found for Cr_xN coatings with increasing chamber pressure from 70 nm·min^{-1} at 300 mPa to 115 nm·min^{-1} at 900 mPa. On the one hand, these results correlate with the trend that at low pressures there is less ionization and, therefore, a lower deposition rate is observed [32]. On the other hand, the deposition rate could further decline with pressure as a result of resputtering and decrease of mean free path in the deposition chamber [33,34]. Benhenda et al. [35] found that the deposition rate first increases and then decreases with increasing pressure. Furthermore, phase composition could also be affected by pressure. Hones et al. [36] indicated that the Cr_2N phase has a higher growth rate than the CrN phase.

Table 1. WDS measurements obtained for the Cr_xN coatings at various pressures.

Element (at. %)	Pressure, mPa		
	300	600	900
Cr	59	62	66
N	41	38	34

3.2. Gas-Phase Hydrogenation

Gas-phase hydrogenation was carried out to investigate hydrogen resistance properties of the Cr_xN coatings deposited on the IN718 alloy, along with changing mechanical and tribological properties after high-temperature hydrogen exposure. The decrease in hydrogen pressure in the chamber indicates that the absorption process is taking place. The slope of the curves shows the hydrogen absorption rates of the samples in Figure 2. The absorption curves are not linear: hydrogen absorption rate gradually decreases with hydrogenation time and tends to saturate when the concentration of absorbed hydrogen is maximal for given temperature and pressure conditions.

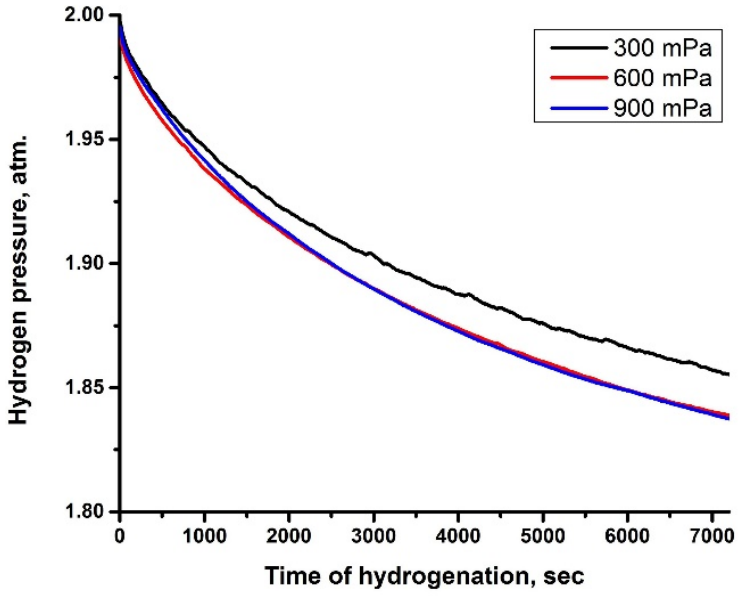

Figure 2. Hydrogen pick-up curves of IN718 with Cr_xN coatings for hydrogenation at 600 °C.

The lowest hydrogen absorption was observed for the Cr_xN coating deposited at 300 mPa, which exhibits dense columnar structure. The absorption rate strongly depends on the kinetics of

hydrogen adsorption on the surface and hydrogen permeation through the coating. These data indicate that the dense structure of the coatings is preferential for hydrogen permeation resistant coatings. Furthermore, the difference in hydrogen absorption could be associated with the changing crystalline structures of the coatings.

3.3. X-ray Diffraction

In the Cr–N system, three solid phases exist: the solid interstitial solution body centered cubic Cr(N), hexagonal Cr_2N, and face centered cubic CrN [31,37]. Wei et al. [37] reported that body centered cubic Cr(N) phase could be formed exclusively at a low nitrogen partial pressure (less than 8%), corresponding to coatings with N concentration $\leq$ 25 at. %. Figure 3a,b show the phase evolution in the Cr_xN films deposited at different pressures obtained by means of X-ray diffraction before and after hydrogenation. With increasing working pressure an evident trend of phases changing from mixed hexagonal Cr_2N and face centered cubic CrN structure to approximately stoichiometric Cr_2N is visible. Three dominant reflections, Cr_2N (113), (111), and CrN (200) occur in the coating deposited at 300 mPa. The reflections of CrN (200) and Cr_2N (200) decline at higher working pressure, while Cr_2N (110) and (111) become dominant reflections (Figure 3a). The increase in the intensity of Cr_2N (110) and (111) reflections with higher working pressure is due to the increase in deposition rate favoring preferential growth along the (111) orientation [18,23]. The appearance of Cr_2N (113) and (300) reflections is related to the enhanced mobility of adatoms on the film surface at high deposition temperatures [23].

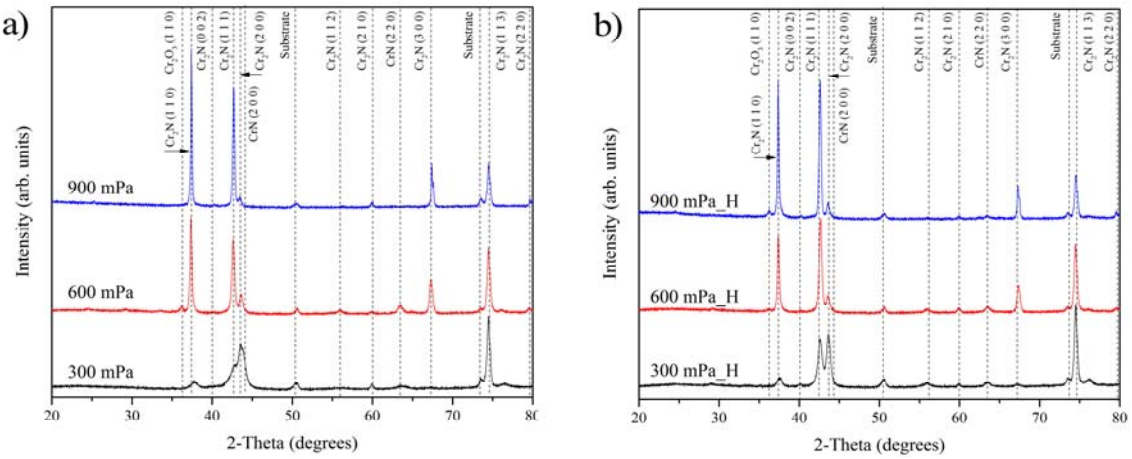

Figure 3. XRD of Cr_xN coatings deposited at different pressures (**a**) before; and (**b**) after hydrogenation.

After hydrogenation, the phase composition remains stable and no new phase occurs. XRD results show that the coating deposited at 300 mPa with the lowest hydrogen absorption has a mixed hcp-Cr_2N and c-CrN structure. Thus, the cubic CrN phase, formed at lower working pressure with its denser structure could improve the barrier properties against hydrogen permeation. Similar results were reported by Tamura et al. for the BN coatings, where coatings containing mixed cubic and hexagonal BN phases were effective in reducing the rate of hydrogen permeation [29]. It could be concluded that the presence of the c-CrN structure is preferable for hydrogen permeation resistant coatings due to a higher packing density of the cubic structure in comparison to the hexagonal structure [38]. Furthermore, preferred orientation of the deposited films strongly depends on the working pressure and could influence mechanical properties and hydrogen permeation, also [39,40].

3.4. Depth Distribution of Elements

Figure 4 shows the depth distribution of elements in the samples before and after hydrogen exposure at 600 °C and 2 atm hydrogen pressure for 2 h. A uniform distribution of the elements Cr and N is observed through the depth of the as-deposited Cr_xN coatings.

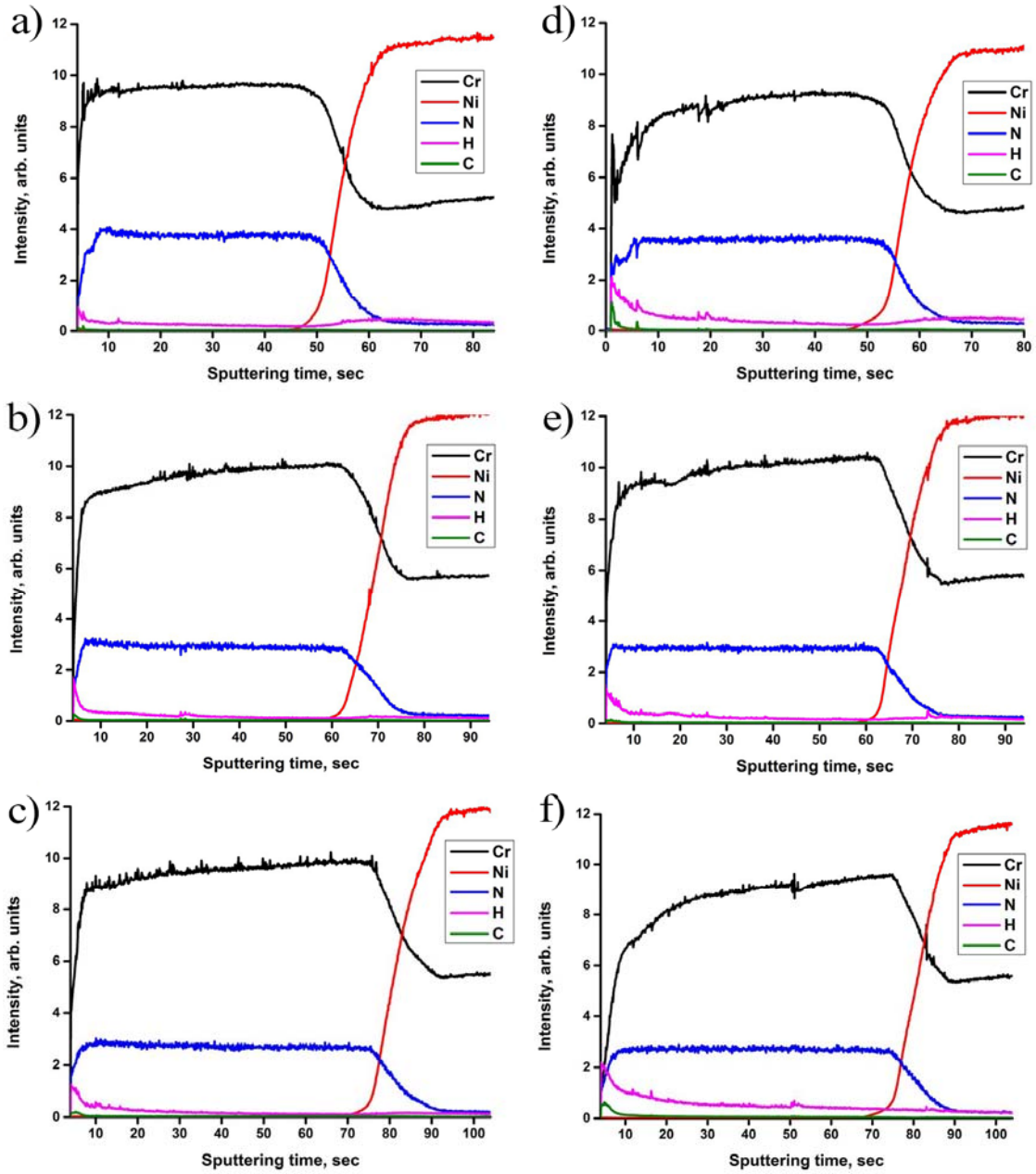

Figure 4. GDOES profiles of elements at (**a**) 300 mPa; (**b**) 600 mPa; (**c**) 900 mPa as-deposited; and (**d**) 300 mPa; (**e**) 600 mPa; (**f**) 900 mPa hydrogen exposed Cr_xN coatings on the IN718 substrates.

The Cr to N ratio increases with pressure. These results are in agreement with the WDS measurements. Fluctuations of the signal intensities in the initial stage are associated with surface contaminations. The hydrogen concentration in the as-deposited coatings is at the same low level, like in the bulk IN718 alloy, which is typically only a few ppm.

After hydrogen exposure, the hydrogen concentration in the coatings does not change significantly (Figure 4d–f). However, hydrogen is trapped at the surface and decreases monotonically with increasing depth to the value of the bulk alloy. Despite low hydrogen values in the GDOES profiles, a large amount of hydrogen is absorbed by the samples during gas-phase hydrogenation (see Figure 2). The reason for such low hydrogen concentration in coatings and substrate is the hydrogen evacuation from the chamber while the samples were still hot. Thus, hydrogen was desorbed during final cooling. Comparison of the results shows that after hydrogen exposure and slow cooling, concentration and

distribution of the residual hydrogen is similar for the coatings deposited at different pressures. These measurements indicate that the absorbed hydrogen does not form strong chemical bonds with the coating elements at these conditions. This result was also confirmed by XRD.

3.5. Mechanical Properties

The mechanical properties of the coatings were characterized by measuring hardness (*H*) and elastic modulus (*E*). Values for hardness and elastic modulus of the as-deposited coatings at different pressures decline with increasing chamber pressure from 18.2 GPa (*H*) and 260 GPa (*E*) at 300 mPa to 7.6 GPa (*H*) and 200 GPa (*E*) at 900 mPa (Figure 5). According to literature, the Cr_2N phase has better mechanical properties compared to CrN [18,41]. The mixed Cr_2N + CrN structure deposited at 300 mPa exhibits higher hardness than Cr_2N deposited at 900 mPa. This is likely related to the change in structure and texture within the coatings. The coating deposited at a low pressure exhibits a denser columnar structure than the one deposited at a high pressure. This leads to a lower hardness of the coating due to incompactness of the columnar structure at a higher pressure [39,42]. Furthermore, residual stresses strongly affects the mechanical properties of coatings [43]. The hardness measured for coating deposited at 900 mPa is lower than the one reported in literature for Cr_xN coatings [18]. The Cr_xN films after hydrogen exposure exhibit higher hardness as well as elastic-modulus and reach a maximum of 21 GPa (*H*) and 300 GPa (*E*) for coating deposited at 300 mPa. This result could be explained by invasion of hydrogen atoms in lattice vacancies inducing lattice distortion in crystal lattice and grain boundaries. Such hardening was observed for AlN coatings after hydrogen permeation, also [44]. Furthermore, hydrogen-induced defects could appear after hydrogen interaction with the coating causing the increase in hardness of the coating. Intensive study of the defect structure of the coatings is required to determine the mechanisms of improving hardness.

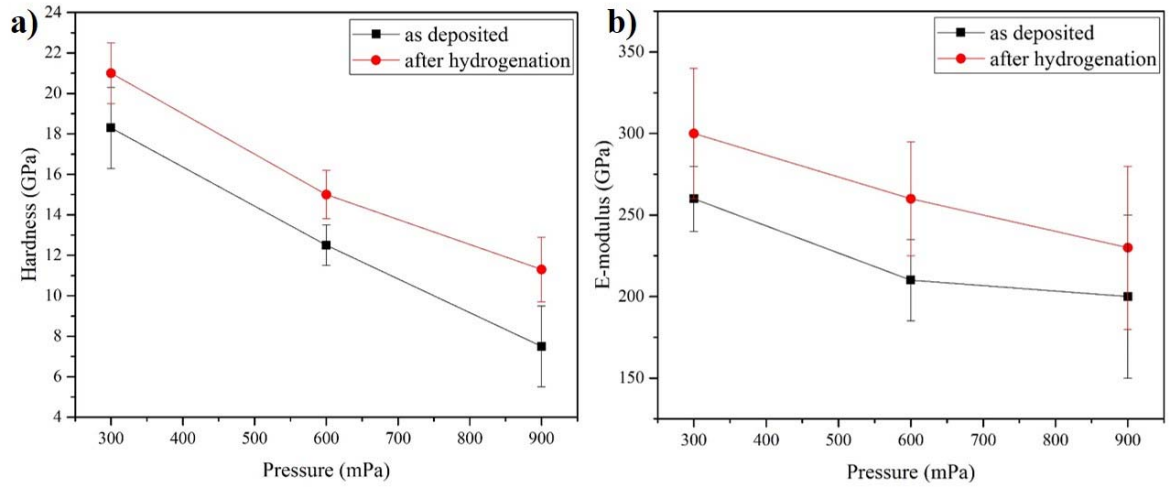

Figure 5. Mechanical properties (**a**) hardness; and (**b**) e-modulus of Cr_xN coatings at various argon pressure as-deposited and after hydrogen exposure.

3.6. Tribology

The results of tribological investigations of the Cr_xN-coated samples before and after hydrogenation are presented in Figure 6. The evolution of the friction coefficient with increasing distance is typical for Cr–N coatings, which is described by Rapoport et al. [45]. As reported previously [39], the friction coefficient for CrN is lower than for Cr_2N. Moreover, according to J. Lin et al. [46] the lowest coefficient was observed in the films containing a mixture of hcp-Cr_2N and c-CrN phases. In our case, the lowest values of CoF 0.35 and 0.34 were achieved for Cr_xN deposited at 300 and 600 mPa, exhibiting a mixture of phases. The friction coefficient increases with pressure up to 0.45 for the coating deposited at 900 mPa. This is likely attributed to the low hardness and highly

porous structure of the coating. The sharp changes in the CoF curves for the deposited coatings at the initial stage are characterized by the ploughing friction arising from the micro asperities of the surface. The small powder-like particles are generated from wear debris after the initial stage of sliding. The entrapped hard wear particles can cause ploughing friction and the occurrence of negligible interlocking effects. With increase in quantity and size of the wear particles, due to third-body hard particles the friction mechanism is ploughing [47,48]. Thus, fluctuations and rapid increase in friction coefficient occur at the end of the test. After hydrogenation, the Cr_xN coatings show (by 20%–30%) a lower friction coefficient for the samples deposited at 300 and 900 mPa, except for the coating deposited at 600 mPa, which average CoF slightly decreased due to another wear character. The best CoF value was 0.25 for the hydrogen exposed Cr_xN coating deposited at 300 mPa. The decrease in the CoF after hydrogenation could be attributed to the increase in hardness and Young's modulus of the coatings. It was shown that the coefficient of friction and wear resistance of coatings depends on the hardness. In particular, there was a decrease in wear resistance of the CrN coatings with a decrease in hardness [49,50]. The coefficient of friction increases when decreasing the hardness of the coating due to an increase of the area of intimate contact between the surface and the counterpart. Until now, the exact reason for the changes in CoF for the deposited coating is not clearly understood and requires further investigations.

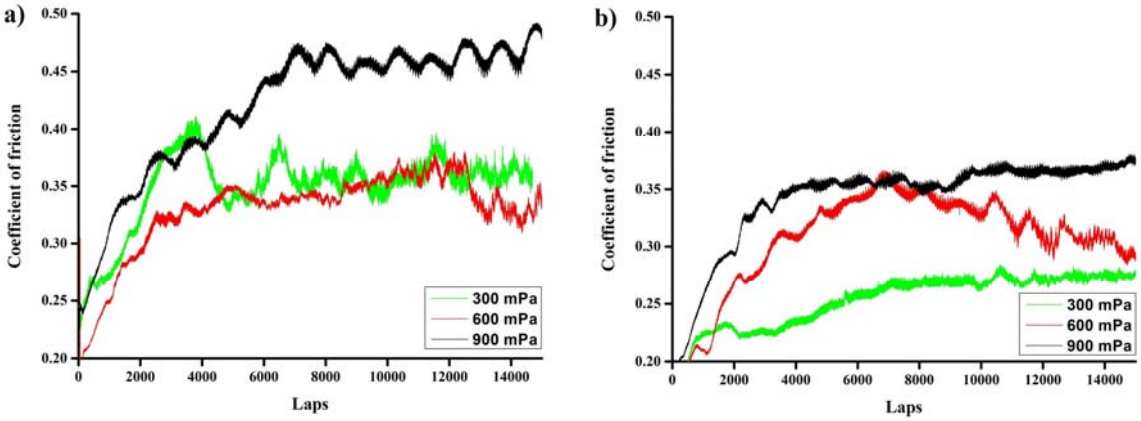

Figure 6. Evolution of friction coefficient for (**a**) as-deposited and (**b**) hydrogen exposed Cr_xN coatings as a function of argon pressure.

4. Conclusions

Cr_xN coatings were deposited on the IN718 substrates at working pressures between 300 and 900 mPa using DC reactive magnetron sputtering. The deposition rate increases with increasing pressure, whereas the Cr/N ratio changes from 1.4 to 1.9. XRD analysis shows the change from mixed hcp-Cr_2N and fcc-CrN structure to approximately stoichiometric Cr_2N with increasing working pressure. Hardness and elastic modulus of the as-deposited coatings decrease with increasing pressure. The hydrogen absorption at 600 °C for all the coatings is similar and the lowest hydrogen absorption rate was observed for the Cr_xN coating deposited at 300 mPa. After hydrogen interaction, the phase composition of the coatings remains stable. It could be concluded that the presence of c-CrN in a mixed structure is preferable for hydrogen permeation resistant coatings, due to the higher packing fraction of cubic structure in comparison to the hexagonal one. After hydrogen exposure, the Cr_xN films exhibit higher hardness as well as elastic-modulus and reach the highest value of 21 GPa (*H*) and 300 GPa (*E*) for the coating deposited at 300 mPa. After hydrogenation, Cr_xN coatings show a lower (by 20%–30%) friction coefficient that favorably affects wear resistance. The best value of CoF was 0.25 for hydrogen exposed Cr_xN coating deposited at 300 mPa.

Acknowledgments: The authors are thankful to Muhammad Naveed for carrying out the deposition process and Sebastian Bolz for performing the WDS measurements. The study was funded by the RFBR under the research project No.16-38-00709. Anton Manakhov also acknowledges the financial support of the Ministry of Education and Science of the Russian Federation in the framework of Increase Competitiveness Program of NUST "MISiS", implemented by a governmental decree dated 16 March 2013, N 211.

Author Contributions: Aleksei Obrosov analyzed the results and prepared the paper with help of Alex A. Volinsky and Anton Manakhov. Alina N. Sutygina and Egor Kashkarov provided hydrogenation, GDOES, and described the results. Sabine Weiß revised the manuscript and directed the work.

Conflicts of Interest: The authors declare no conflict of interest.

References

1. Niu, Y.; Wei, J.; Yu, Z. Microstructure and tribological behavior of multilayered CrN coating by arc ion plating. *Surf. Coat. Technol.* **2015**, *275*, 332–340. [CrossRef]
2. Liu, B.; Deng, B.; Tao, Y. Influence of niobium ion implantation on the microstructure, mechanical and tribological properties of TiAlN/CrN nano-multilayer coatings. *Surf. Coat. Technol.* **2014**, *240*, 405–412. [CrossRef]
3. Uchida, M.; Nihira, N.; Mitsuo, A.; Toyoda, K.; Kubota, K.; Aizawa, T. Friction and wear properties of CrAlN and CrVN films deposited by cathodic arc ion plating method. *Surf. Coat. Technol.* **2004**, *177–178*, 627–630. [CrossRef]
4. Warcholinski, B.; Gilewicz, A. Effect of substrate bias voltage on the properties of CrCN and CrN coatings deposited by cathodic arc evaporation. *Vacuum* **2013**, *90*, 145–150. [CrossRef]
5. Gilewicz, A.; Warcholinski, B.; Myslinski, P.; Szymanski, W. Anti-wear multilayer coatings based on chromium nitride for wood machining tools. *Wear* **2010**, *270*, 32–38. [CrossRef]
6. Wieciński, P.; Smolik, J.; Garbacz, H.; Kurzydłowski, K.J. Failure and deformation mechanisms during indentation in nanostructured Cr/CrN multilayer coatings. *Surf. Coat. Technol.* **2014**, *240*, 23–31. [CrossRef]
7. Sue, J.A.; Perry, J.A.; Vetter, A.J. Young's modulus and stress of CrN deposited by cathodic vacuum arc evaporation. *Surf. Coat. Technol.* **1994**, *68*, 126–130. [CrossRef]
8. Major, L.; Morgiel, J.; Major, B.; Lackner, J.M.; Waldhauser, W.; Ebner, R.; Nistor, L.; van Tendeloo, G. Crystallographic aspects related to advanced tribological multilayers of Cr/CrN and Ti/TiN types produced by pulsed laser deposition (PLD). *Surf. Coat. Technol.* **2006**, *200*, 6190–6195. [CrossRef]
9. Lackner, J.M.; Waldhauser, W.; Berghauser, R.; Ebner, R.; Kothleitner, G. Growth phenomena in room temperature pulsed laser deposited chromium and chromium nitride coatings. *Surf. Coat. Technol.* **2005**, *200*, 387–390. [CrossRef]
10. Kumar, S.; Raju, V.S.; Shekhar, R.; Arunachalam, J.; Khanna, A.S.; Prasad, K.G. Compositional characterization of CrN films deposited by ion beam-assisted deposition process on stainless steel. *Thin Solid Films* **2001**, *388*, 195–200. [CrossRef]
11. Guglya, A.G.; Marchenko, I.G.; Malykhin, D.G.; Neklyudov, I.M. Production of Cr-N films by ion beam-assisted deposition technology: Experiment and computer simulation. *Surf. Coat. Technol.* **2003**, *163–164*, 286–292. [CrossRef]
12. Egawa, M.; Miura, K.I.; Yokoi, M.; Ishigami, I. Effects of substrate bias voltage on projection growth in chromium nitride films deposited by arc ion plating. *Surf. Coat. Technol.* **2007**, *201*, 4873–4878. [CrossRef]
13. Zhang, M.; Kim, K.H.; Xu, F.; Yang, X. Structure and oxidation behavior of compositionally gradient CrN_x coatings prepared using arc ion plating. *Surf. Coat. Technol.* **2013**, *228*, S529–S533. [CrossRef]
14. Chang, Z.K.; Wan, X.S.; Pei, Z.L.; Gong, J.; Sun, C. Microstructure and mechanical properties of CrN coating deposited by arc ion plating on Ti6Al4V substrate. *Surf. Coat. Technol.* **2011**, *205*, 4690–4696. [CrossRef]
15. Tan, S.; Zhang, X.; Wu, X.; Fang, F.; Jiang, J. Comparison of chromium nitride coatings deposited by DC and RF magnetron sputtering. *Thin Solid Films* **2011**, *519*, 2116–2120. [CrossRef]
16. Lee, J.-W.; Kuo, Y.-C.; Wang, C.-J.; Chang, L.-C.; Liu, K.-T. Effects of substrate bias frequencies on the characteristics of chromium nitride coatings deposited by pulsed DC reactive magnetron sputtering. *Surf. Coat. Technol.* **2008**, *203*, 721–725. [CrossRef]
17. Shah, H.N.; Jayaganthan, R.; Kaur, D.; Chandra, R. Influence of sputtering parameters and nitrogen on the microstructure of chromium nitride thin films deposited on steel substrate by direct-current reactive magnetron sputtering. *Thin Solid Films* **2010**, *518*, 5762–5768. [CrossRef]

18. Obrosov, A.; Naveed, M.; Volinsky, A.A.; Weiß, S. Substrate frequency effects on Cr_xN coatings deposited by DC magnetron sputtering. *J. Mater. Eng. Perform.* **2017**, *26*, 366–373. [CrossRef]
19. Odén, M.; Almer, J.; Håkansson, G. The effects of bias voltage and annealing on the microstructure and residual stress of arc-evaporated Cr-N coatings. *Surf. Coat. Technol.* **1999**, *120–121*, 272–276. [CrossRef]
20. Krella, A.; Czyżniewski, A. Cavitation resistance of Cr-N coatings deposited on austenitic stainless steel at various temperatures. *Wear* **2009**, *266*, 800–809. [CrossRef]
21. Odén, M.; Ericsson, C.; Håkansson, G.; Ljungcrantz, H. Microstructure and mechanical behavior of arc-evaporated Cr-N coatings. *Surf. Coat. Technol.* **1999**, *114*, 39–51. [CrossRef]
22. Wan, X.S.; Zhao, S.S.; Yang, Y.; Gong, J.; Sun, C. Effects of nitrogen pressure and pulse bias voltage on the properties of Cr-N coatings deposited by arc ion plating. *Surf. Coat. Technol.* **2010**, *204*, 1800–1810. [CrossRef]
23. Shah, H.N.; Jayaganthan, R.; Kaur, D. Effect of sputtering pressure and temperature on dc magnetron sputtered CrN films. *Surf. Eng.* **2010**, *26*, 629–637. [CrossRef]
24. Sjoberfg, G.; Cornu, D. Hydrogen Embrittlement of Cast Alloy 718 Effects of Homogenization, Grain Size and δ-Phase. In *Superalloys 718, 625, 706 and Various Derivatives (2001)*; The Minerals, Metals & Materials Society (TMS): Pittsburgh, PA, USA, 2001; pp. 679–690, ISBN: 0873395107, 9780873395106.
25. Oliver, W.C.; Pharr, G.M. An improved technique for determining hardness and elastic modulus using load and displacement sensing indentation experiments. *J. Mater. Res.* **1992**, *7*, 1564–1583. [CrossRef]
26. Obrosov, A.; Gulyaev, R.; Zak, A.; Ratzke, M.; Naveed, M.; Dudzinski, W.; Weiß, S. Chemical and morphological characterization of magnetron sputtered at different bias voltages Cr-Al-C coatings. *Materials* **2017**, *10*, 156. [CrossRef]
27. Kashkarov, E.B.; Nikitenkov, N.N.; Sutygina, A.N.; Bezmaternykh, A.O.; Kudiiarov, V.N.; Syrtanov, M.S.; Pryamushko, T.S. Hydrogenation behavior of Ti-implanted Zr-1Nb alloy with tin films deposited using filtered vacuum arc and magnetron sputtering. *Appl. Surf. Sci.* **2017**. [CrossRef]
28. Wang, Q.; Zhou, F. Progress in tribological properties of nano-composite hard coatings under water lubrication. *Lubricants* **2017**, *5*, 5. [CrossRef]
29. Tamura, M.; Noma, M.; Yamashita, M. Characteristic change of hydrogen permeation in stainless steel plate by BN coating. *Surf. Coat. Technol.* **2014**, *260*, 148–154. [CrossRef]
30. Sidelev, D.V.; Bleykher, G.A.; Krivobokov, V.P.; Koishybayeva, Z. High-rate magnetron sputtering with hot target. *Surf. Coat. Technol.* **2016**, *308*, 168–173. [CrossRef]
31. McHale, A.E. Borides, carbides, and nitrides. In *Phase Equilibria Diagrams: Phase Diagrams for Ceramists*; American Ceramic Society: Washington DC, USA, 1994; Volume X, ISBN: 9780944904749.
32. Eufinger, K.; Janssen, E.N.; Poelman, H.; Poelman, D.; De Gryse, R.; Marin, G.B. The effect of argon pressure on the structural and photocatalytic characteristics of TiO_2 thin films deposited by d.c. Magnetron sputtering. *Thin Solid Films* **2006**, *515*, 425–429. [CrossRef]
33. Klabunde, F.; Löhmann, M.; Bläsing, J.; Drüsedau, T. The influence of argon pressure on the structure of sputtered molybdenum: From porous amorphous to a new type of highly textured film. *J. Appl. Phys.* **1996**, *80*, 6266–6273. [CrossRef]
34. Mergel, D.; Buschendorf, D.; Eggert, S.; Grammes, R.; Samset, B. Density and refractive index of TiO_2 films prepared by reactive evaporation. *Thin Solid Films* **2000**, *371*, 218–224. [CrossRef]
35. Benhenda, S.; Guglielmacci, J.M.; Gillet, M. Characterization of tin films grown by reactive d.c. Triode sputtering onto copper substrates. *Mater. Sci. Eng. B* **1995**, *34*, 36–41. [CrossRef]
36. Hones, P.; Sanjines, R.; Levy, F. Characterization of sputter-deposited chromium nitride thin films for hard coatings. *Surf. Coat. Technol.* **1997**, *94*, 398–402. [CrossRef]
37. Wei, G.; Rar, A.; Barnard, J.A. Composition, structure, and nanomechanical properties of DC-sputtered CrN_x ($0 \leq x \leq 1$) thin films. *Thin Solid Films* **2001**, *398–399*, 460–464. [CrossRef]
38. Ellis, A.B. *Teaching General Chemistry: A Materials Science Companion*; American Chemical Society: Washington DC, USA, 1993; ISBN: 978-0841227255.
39. Han, S.; Lin, J.H.; Wang, G.H.; Shih, H.C. The effect of preferred orientation on the mechanical properties of chromium nitride coatings deposited on SKD11 by unbalanced magnetron sputtering. *Mater. Lett.* **2003**, *57*, 1202–1209. [CrossRef]
40. Zhou, T.; Liu, D.; Zhang, Y.; Ouyang, T.; Suo, J. Microstructure and hydrogen impermeability of titanium nitride thin films deposited by direct current reactive magnetron sputtering. *J. Alloys Compd.* **2016**, *688*, 44–50. [CrossRef]

41. Zhao, Z.B.; Rek, Z.U.; Yalisove, S.M.; Bilello, J.C. Phase formation and structure of magnetron sputtered chromium nitride films: In-situ and ex-situ studies. *Surf. Coat. Technol.* **2004**, *185*, 329–339. [CrossRef]
42. Bull, S.J.; Rickerby, D.S. Compositional, microstructural and morphological effects on the mechanical and tribological properties of chromium nitrogen films. *Surf. Coat. Technol.* **1990**, *43*, 732–744. [CrossRef]
43. Shah, H.N.; Chawla, V.; Jayaganthan, R.; Kaur, D. Microstructural characterizations and hardness evaluation of d.c. Reactive magnetron sputtered CrN thin films on stainless steel substrate. *Bull. Mater. Sci.* **2010**, *33*, 103–110. [CrossRef]
44. Wang, J.; Li, Q.; Xiang, Q.-Y.; Cao, J.-L. Performances of AlN coatings as hydrogen isotopes permeation barriers. *Fusion Eng. Des.* **2016**, *102*, 94–98. [CrossRef]
45. Rapoport, L.; Moshkovich, A.; Perfilyev, V.; Lapsker, I.; Kugler, M.; Kailer, A.; Renz, A.; Hollstein, T. High temperature friction behavior of CrV_xN coatings. *Surf. Coat. Technol.* **2014**, *238*, 207–215. [CrossRef]
46. Lin, J.; Wu, Z.L.; Zhang, X.H.; Mishra, B.; Moore, J.J.; Sproul, W.D. A comparative study of CrN_x coatings synthesized by dc and pulsed dc magnetron sputtering. *Thin Solid Films* **2009**, *517*, 1887–1894. [CrossRef]
47. Godet, M. The third-body approach: A mechanical view of wear. *Wear* **1984**, *100*, 437–452. [CrossRef]
48. Singer, I.L. How third-body processes affect friction and wear. *MRS Bull.* **1998**, *23*, 37–40. [CrossRef]
49. Moore, A.J.W.; Tegart, W.J.M. Relation between friction and hardness. *Proc. R. Soc. Lond. Ser. A Math. Phys. Sci.* **1952**, *212*, 452–458.
50. Mo, J.L.; Zhu, M.H. Tribological characterization of chromium nitride coating deposited by filtered cathodic vacuum arc. *Appl. Surf. Sci.* **2009**, *255*, 7627–7634. [CrossRef]